Nano-Structures & Nano-Objects 29 (2022) 100841

Contents lists available at ScienceDirect

Nano-Structures & Nano-Objects

journal homepage: www.elsevier.com/locate/nanoso

Silver nanocolloid generation using dynamic Laser Ablation Synthesis in Solution system and drop-casting

Éanna McCarthy [a], Sithara Pavithran Sreenilayam [a,*], Oskar Ronan [b], Hasan Ayub [a], Ronan McCann [a,c,d], Lorcan McKeon [b], Karsten Fleischer [a], Valeria Nicolosi [b], Dermot Brabazon [a,c,d]

[a] I-Form, Advanced Manufacturing Research Centre, & Advanced Processing Technology Research Centre, School of Mechanical and Manufacturing Engineering, Dublin City University, Glasnevin, Dublin-9, Ireland
[b] I-Form and AMBER Research Centers, School of Chemistry, Trinity College Dublin, Dublin 2, Ireland
[c] National Centre for Plasma Science and Technology, Dublin City University, Glasnevin, Dublin 9, Ireland
[d] National Center for Sensor Research (NCSR), Dublin City University, Glasnevin, Dublin 9, Ireland

ARTICLE INFO

Article history:
Received 7 August 2021
Received in revised form 21 December 2021
Accepted 17 January 2022

Keywords:
Silver nanoparticle
Laser ablation
Nanocolloid
Drop-casting TEM
FESEM

ABSTRACT

Conductive inks allow for low cost and scalable deposition of conductive tracks and patterns for printed electronics. Metal nanoparticle colloids are a novel form for producing conductive inks. Laser Ablation Synthesis in Solution (LASiS) is a "green" method for the production of metal nanoparticle colloids without the need for environmentally hazardous chemicals, however the method has typically been limited by its low production rates. This study reports on the generation of an additive free silver nanocolloid with maximized productivity using a flow-based LASiS system and its characterization using dynamic light scattering, UV–VIS, transmission electron microscopy and field emission scanning electron microscopy. The productivity of the LASiS silver nanoparticle (size ~34 ± 5 nm) was ~0.9 mg mL^{-1}. While the flow-based system achieves high laser ablation rates in the mass of nanomaterial generated per unit time, the volume of liquid required for the flow leads to relatively low concentrations. Therefore, in this work, LASiS concentrated ink was formulated *via* a centrifugal method, which was then drop-cast and heat treated to produce a conductive silver layer. Centrifuging to concentrate the ink was shown to be a necessary step to achieve good results, with the lowest resistance across the drop-cast material of 60.2 Ω after annealing.

1. Introduction

Conductive inks have been extensively investigated in recent years due to their popularity in flexible electronics and printing technologies [1]. There has been a growing demand for highly conductive printable tracks in various fields, including flexible displays, wearable devices, smart packaging, thin-film transistors, smart textiles and solar cells [1,2]. Printed electronics (PEs) offer several attractive characteristics, including lower costs, optical transparency, light weight and increased production of devices on different flexible substrates, including polymers, paper, glass *etc.*, at large scales [1]. Due to their application in flexible PEs, the global market for conductive inks has grown significantly in recent years. Estimates predict that the conductive ink market will reach 3.7 billion USD by 2025, up from 3.0 billion USD in 2020 [3]. The main element of conductive inks are the functional materials, for example, metal nanoparticles (NPs) [4], organic/metallic compounds [5], carbon [6], conductive polymers [7], and metal precursors [8]. Metal NPs (*e.g.*, copper (Cu) [9], gold (Au) [10] and silver (Ag) [11–13]) are most commonly used in conductive inks since their resistivity is comparable to that of the bulk material. These conductive particles are suspended in a liquid medium, allowing them to act as an ink, being a liquid at room temperature. This provides ease of handling and printing compared with molten metal, and the inks can form conductive patterns when deposited and dried.

Chemical and physical methods are commonly used to generate NPs. Evaporation condensation and laser ablation are two important physical processes that are implemented. Laser Ablation Synthesis in Solution (LASiS) is a physical technique that synthesizes NPs in liquid media [15–22] using laser energy, unlike wet-chemical synthesis methods which use environmentally harmful reducing agents. The process involves a pulsed laser focused on the surface of a solid target in a liquid environment, ablating material from the target and producing ligand free NPs. In 1987, Patil et al. first explored material synthesis at a solid–liquid interface using a pulsed laser (ruby laser with a pulse

* Corresponding author.
E-mail address: sithara.sreenilayam@dcu.ie (S.P. Sreenilayam).

https://doi.org/10.1016/j.nanoso.2022.100841
2352-507X/

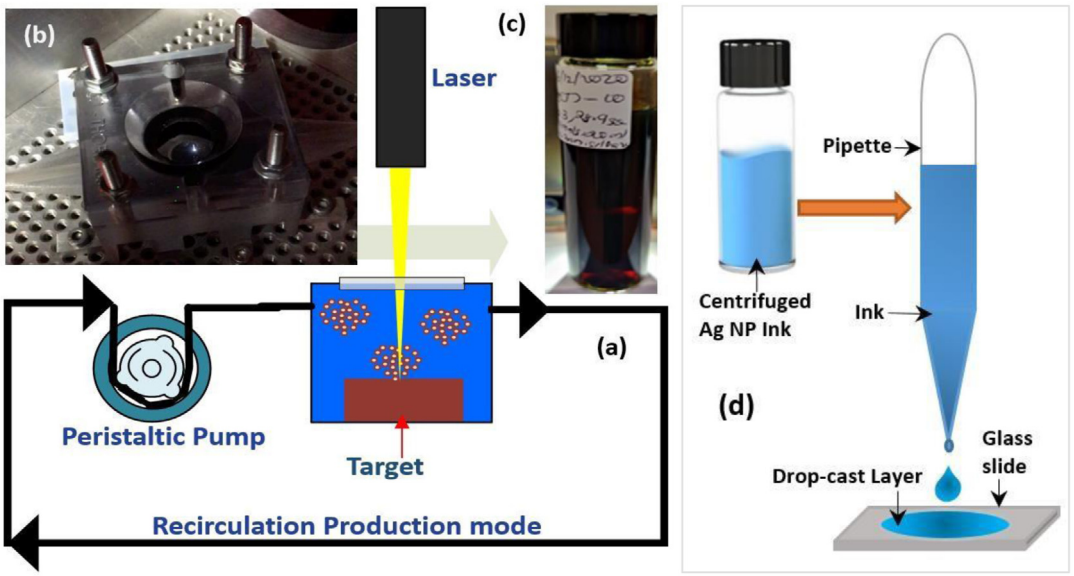

Fig. 1. (a) Laser Ablation Synthesis in Solution (LASiS) set-up for the production of Ag NPs in DI water: recirculation production mode. [14] (b) Laser irradiation (wavelength, $\lambda = 1064$ nm) of Ag bulk target inside a 3D printed flow-cell. (c) Ag NPs produced *via* LASiS technique in 20 ml DI water. (d) schematic of centrifuged Ag NP ink drop-cast on a glass slide.

width of 30 ns) by generating metastable iron oxide from an iron substrate in water [23]. Later in 1993, Neddersen et al. reported the generation of organic solvent and water based stable colloids, without any ionic or organic species, from metal targets such as Cu, Pt, Pd, Au and Ag *via* laser ablation [24]. The LASiS technique has been used for the generation of highly pure nanostructures in aqueous solutions at room temperature and normal pressure conditions since 2000 [14,25–28] and several NP colloids of metals (*e.g.,* Ag [29], Cu [29,30] and Au [31]), polymers [32], semiconductors (*e.g.*, silicon carbide (SiC) [33], silicon (Si) [34] and zinc oxide (ZnO) [35]) and carbon (C) [36] have been synthesized using this method.

NP-based inks enable the development of novel applications due to the different possible material combinations and properties. Among the conductive inks, Ag NP based ink is widely used in various applications owing to its high thermal conductivity and printability. This material conducts well in both its oxide and metallic states, so the technological risk associated with its use is low. Due to the high conductivity of the ink, lower volumes of ink will be needed to produce good quality PE devices. During the past few decades, LASiS has been widely investigated for nanomaterial production in liquid, with a view to enabling cost-effective PE conductive ink formulation. In this simple method, several experimental parameters, including laser energy, repetition rate, laser wavelength, solvent, *etc.* can easily be adjusted to determine size of the NPs, their stability in liquids and the productivity of the NPs [37]. The properties of colloidal solutions have a strong influence on the size, shape, production rate and polydispersity of NPs [38]. In PEs, the NP productivity plays a crucial role, since the NP concentration and size in the colloids heavily influence the conductivity of the printed track and thereby the quality of the device. Although the commonly used static LASiS technique is simple, its low productivity hinders acceptance of this method within manufacturing industries [39]. In this study, the use of a high production rate, dynamic flow-based LASiS system to produce Ag NP colloids for conductive inks and their drop-cast pattern characterization is reported. The resistance properties of the functional inks were studied with the drop-cast technique prior to using them in inkjet or aerosol jet printing applications. The volume of liquids required for flow-based production may lead to low concentrations, despite the high production rates. After the production of the Ag nanocolloids *via* LASiS, they were centrifuged to increase their concentration, as ink conductivity is highly dependent on the ink concentration. The as-produced and centrifuged Ag nanocolloids were deposited on glass slides by drop-casting and the resistance was measured in-situ during heating, in order to determine the as-deposited resistance, the temperature required for heat-treatment and the reduced resistance achievable after heating. This achieves the objective of establishing the suitability of the LASiS method for ink production for PE application, whether concentration and the correct parameters and effect for annealing are necessary.

2. Experimental details

2.1. Materials

Ag discs (99.99+% metals basis, sourced from Goodfellow Cambridge Ltd) were used as the target material in the LASiS process. The DI water for nanocolloid formation was purchased from Merck (LC-MS Grade LiChrosolv).

2.2. Method: Laser ablation synthesis in solution and Ag NP generation

A schematic of the experimental LASiS dynamic flow based set-up used for the generation of Ag NPs is shown in Fig. 1a [14]. The laser ablation of the Ag target (8 mm diameter) was carried out using a micro-machining low-power picosecond Nd: YAG laser (WEDGE HF 1064, BrightSolutions, Italy), with a wavelength (λ) of 1064 nm. The laser beam was focused on the Ag target to a spot diameter of 100 μm and scanned over the target surface using a 2D scanning galvanometer (Raylase SS-12) at a scan speed of 2.6 mm/s in an Archimedean spiral pattern (see Fig. 2a). Prior to the laser ablation, the Ag target was mechanically polished using silicon carbide paper up to 1200 grit, cleaned in an ultrasonic bath for 20 min and then thoroughly rinsed with DI water.

The pulse repetition frequency of the laser was 20 kHz and the duration of the laser ablation was 30 min. The Ag target was mounted within the centre of a 3D-printed custom-designed flowcell (Fig. 1b) kept on a 1D-nanopositioning stage (M-404 4PD, PI, Germany) and a 2 mm ID PTFE piping network was used to

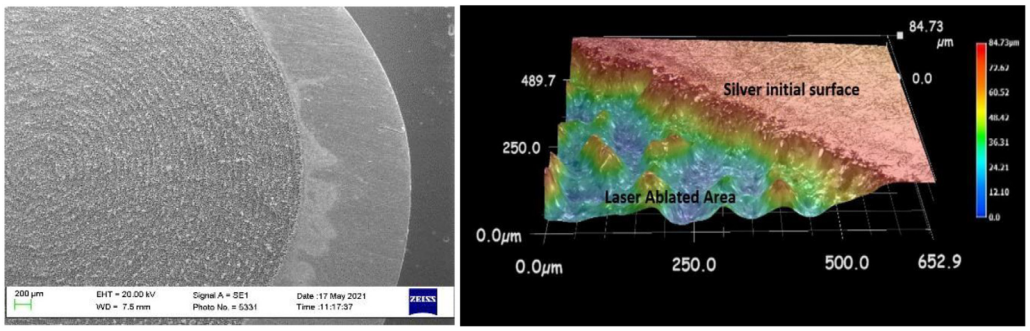

Fig. 2. (a) Scanning electron microscopy (SEM) and (b) 3D optical profilometer images of the bulk Ag target after 30 min laser ablation.

circulate 20 ml DI water. The flow of the DI water through the piping network was controlled by a peristaltic pump (Isamatic MCPV510, Millipore Ltd.) which can control the liquid flow rate at 10–400 mL min^{-1}. In this work, the DI water flow rate was kept at 100 mL min^{-1}. The top and bottom parts of the 3D printed flow-cell was made up of photopolymers, VeroWhitePlus (RGD835) and TangoBlack (FLX973), and fabricated using a Stratasys Object 260 Connex1 3D printer (Fig. 1b) [14] which uses the Polyjet 3D printing technology. This printer allows printing of 3D models as large as 255 × 252 × 200 mm (build area). The machine has a 16-micron layer accuracy and 14 photopolymers to simulate a range of material characteristics and create 3D models. The use of flow-cell limits occluding of the surface from the beam by the ablated material (due to the produced particles being moved by the flow) [16,17,40]. The process parameters of the laser power, stage height, laser beam scan speed, raster pattern and laser repetition rate were controlled using the National Instruments LabVIEW programme. After 30 min of ablation using a 2.6 mm sec^{-1} laser beam scan speed in an Archimedean spiral pattern, the target surface was examined using both Zeiss EVO LS15 scanning electron microscopy (SEM) (Fig. 2a) and a 3D optical microscope from Keyence 2000 (Fig. 2b). The silver target sample used for post ablation microscopic characterization was ultrasonicated for 30 min to clean the surface well. The depth of the spiral on the Ag target is 61 μm from the initial Ag target surface after 30 min of laser ablation (Fig. 2b).

An optical absorption spectrum of the LASiS Ag colloid was recorded in a quartz cuvette (10 mm path length, Helma) with a Varian Cary 50 UV–VIS spectrophotometer (scan range 200–1200 nm with a scan rate of 600 nm min^{-1}). The optical spectrum was corrected for DI water absorption by subtracting the DI water contribution from the recorded UV–VIS spectrum. This analytical technique measures the amount of discrete wavelengths of visible or UV light that are transmitted through or absorbed by a sample in comparison to a reference sample. The size distribution and shape of the as produced Ag NPs were analysed using dynamic light scattering (DLS, NANO-flex® 180° DLS Size, Microtrac Ltd.) and a transmission electron microscope (TEM, FEI Titan (S)TEM (FEI, USA) with beam energy of 300 keV). DLS is a commonly used established method enabling nanoparticle analysis and characterization in solution in a size range 0.3 nm - 10 μm. Light scattering occurs in all directions when it hits smaller particles having a size below 250 nm. In the DLS technique, the scattering intensity of the laser beam in a colloid fluctuates over time due to the Brownian motion of the particles. This undergoes either destructive or constructive interference by the surrounding particles. The Brownian movement of the particle in a colloid is modelled by the Stokes–Einstein Eq. as:

$$D_h = \frac{k_B T}{3\pi \eta D_t} \quad (1)$$

where D_h is the hydrodynamic diameter of the nanoparticles, η is the dynamic viscosity, D_t is the translational diffusion coefficient, k_B is Boltzmann's constant and T is the thermodynamic temperature. The Ag colloidal sample for TEM was prepared by depositing a drop of Ag suspension on a lacey carbon 400 mesh copper (Cu) grid (01896-F, TED PELLA Inc.). The centrifuged-concentrated Ag NP colloid was characterized using a field emission scanning electron microscope (FESEM, Hitachi S5500 Field Emission SEM). This instrument is capable of imaging in scanning transmission electron microscopy (STEM) and is commonly used for nanoparticle imaging. The dark field and bright field Duo-STEM detector allows simultaneous observation of dark field and bright field STEM images. The FE-SEM characterization of the centrifuge concentrated LASiS silver colloid was carried out by depositing a drop of the colloidal sample on a polished silicon substrate and drying it in air.

The productivity of the Ag NPs in the LASiS system was ∼0.9 mg mL^{-1} for the parameters 20 kHz pulse repetition frequency, 2.6 mm s^{-1} scan speed and 30 min process duration (Fig. 1c). It was calculated manually by measuring the Ag target weight before and after the laser ablation process.

2.3. Method: centrifuging ink

20 ml of Ag nanocolloid produced *via* LASiS in the recirculation production mode (Fig. 1b) was centrifuged in a Hettich Lab Technology™ Universal 320 Benchtop Centrifuge for 10 min at 10000 rpm. After centrifuging, 15 ml of the supernate was removed, and the remaining solution was ultrasonicated for one hour and 30 min to re-suspend the settled Ag NPs.

2.4. Method: dropcasting and heat-treatment

The inks were drop-cast onto glass slides as shown in the schematic Fig. 1d by depositing 0.5 mL of ink from a pipette and allowing it to spread naturally and dry in air (inset figures of Figs. 6 and 7). This was performed three times consecutively on the same spot to produce the deposited layers. The liquid was allowed to spread naturally, forming elliptical or circular layers of ∼1520 mm diameter, with an estimated liquid layer thickness of roughly 1.6–2.8 mm. For the 0.9 mg mL^{-1} concentration as-produced LASiS silver colloid, there would be a total of 1.35 mg of Ag NPs deposited in the drop-casting procedure. Treating the layer as a cylindrical disc, a dried layer thickness of roughly 0.4–0.8 μm would be estimated. For the centrifuge concentrated ink, where 75% of the supernate was removed, the concentration should be 4 times that of the as-produced sample, 3.6 mg mL^{-1}, which would give about 5.4 mg total deposited mass of Ag NPs after the drop-casting procedure. This would give an estimated dried layer thickness of roughly 1.6–2.9 μm. Ag liquid conductive

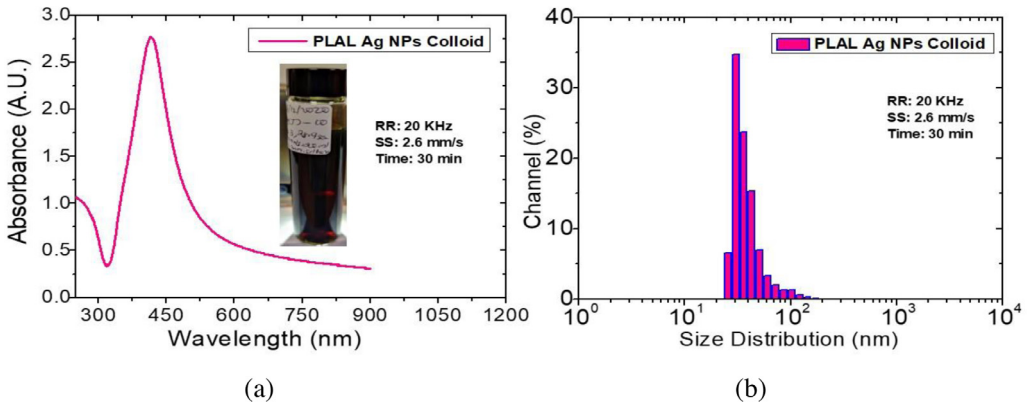

Fig. 3. (a) UV–VIS absorbance as a function of wavelength and (b) average particle size distribution from the DLS technique for the Ag NP colloids generated in the dynamic LASiS system with 100 mL min^{-1} liquid flow rate.

paint (sourced from Radionics, RS Pro Conductive Paint) was applied on either side of the drop-casted layer, as shown in Figs. 6 and 7a, to make contacts to which a multimeter could be applied without damaging the deposited silver layers. The glass slides were placed on a resistive heater in a sealed chamber with a nitrogen flow and the temperature set-up was ramped up and down in stages while measuring the resistance in situ. The temperature ranges were 45–90, 65–110, 85–130, 105–150, 125–170, 145–190, 165–210, 185–230 and 205–250 °C (see Figs. 6 and 7). By observing the hysteresis in each stage, the temperature at which the resistance begins to permanently change could be observed. After heat treatment, the samples were allowed to cool in the nitrogen flow, then the first three heating stages (45–90, 65–110 and 85–130 °C (see Fig. 7b)) were repeated to observe the permanently changed resistance behaviour.

3. Results and discussions

3.1. Ag nanocolloid characterization

The UV–VIS absorption spectrum of the as-produced LASiS Ag colloid (Fig. 3a) shows the presence of an absorption peak in the ∼400 nm wavelength region, confirming the Ag NP formation in DI water. The optical characteristics of the Ag NPs are strongly influenced by their diameter, *i.e.* with an increase in the NP size, the absorption peak will move towards a higher wavelength region. For larger particles, particularly above 80 nm in size, a secondary absorption peak appears at a lower wavelength region as a result of quadrupole resonance in addition to the primary dipole resonance [41]. When the Ag NPs destabilize, the intensity of the original absorption will decrease due to the depletion of stable NPs, broadening the peak or leading to the formation of another secondary absorption peak at a longer wavelength due to aggregation of the NPs. As the optical characteristics are greatly affected by NP aggregation, this UV–VIS technique can be used to monitor Ag NP colloidal stability over time. The stability of conductive inks is of great concern when they are used in PE applications.

The DLS Ag NP size distribution plot is shown in Fig. 3b, which is determined by calculating the random fluctuations in the monochromatic polarized laser light intensity that is scattered by the Ag colloidal solution. The as-produced LASiS Ag colloidal solution exhibits a singular peak distribution with an average particle size diameter of 34 ± 5 nm.

The particle size distribution and the morphology of the Ag NPs produced by LASiS were further confirmed by TEM. Fig. 4 shows the TEM images of Ag NPs generated *via* LASiS in 20 mL DI water. The LASiS Ag NPs deposited on the lacey carbon grid were single or in clusters. It was found that the diameter of the individual Ag NPs was ∼30 nm in the test colloidal solution (Fig. 4).

The size and morphology of the Ag NPs in the centrifuge-concentrated colloid (Fig. 5a) were characterized using FESEM (Fig. 5b, c). The FESEM sample was prepared by depositing a drop of solution on a polished silicon substrate and drying it in air. SEM images of the Ag NPs in the concentrated colloid recorded using a secondary electron (SE) detector (Fig. 5b) and a Brightfield (BF) detector (Fig. 5c) show that the Ag NPs are mostly spherical in shape and appear both as single particles as well as in the form of aggregates.

3.2. Drop-casting and characterization

Drop-casting is a commonly used convenient and fast coating technique for the generation of small area films [42]. In this cost-effective method, droplets containing the particles (*e.g.,* NPs, nanotubes, *etc.*) of interest are directly deposited using a capillary tube on the selected substrate or electrode surface, followed by evaporation of the solvent. A fast initial study of functional ink conductivity properties can be done with this technique prior to using the functional ink in inkjet or aerosol jet printing applications. In drop-cast patterns, the conductivity is related to the NP distribution, in addition to the properties of the NPs themselves. Inset pictures of Figs. 6 and 7 show the drop-cast patterns on glass plates made using the as-produced (Fig. 6 inset) and centrifuge-concentrated (Fig. 7a inset) LASiS Ag colloids. The drop-cast pattern formed by the Ag colloids is in the shape of an ellipse, while the centrifuge-concentrated colloid produces patterns that are almost circular in shape. The momentum of the droplet influences how the ink spreads on the chosen substrate. Droplet jetting and spreading on the substrate is usually described in terms of dimensionless physical constants, such as the Weber number, *We*, (which represents the ratio between the drop inertial forces and surface tension forces) and Reynolds number, *Re*, (which represents the ratio between the drop inertial forces and viscous forces) [43]. Thus, droplet spreading is controlled by ink density, viscosity, surface tension, impinging velocity and droplet size *via We* and *Re* numbers, as well as substrate surface wetting characteristics.

The resistance *vs.* temperature plot measured in situ for the as-produced Ag ink is presented in Fig. 6. The initial resistance for this sample was out of the multimeter's measurement range. The

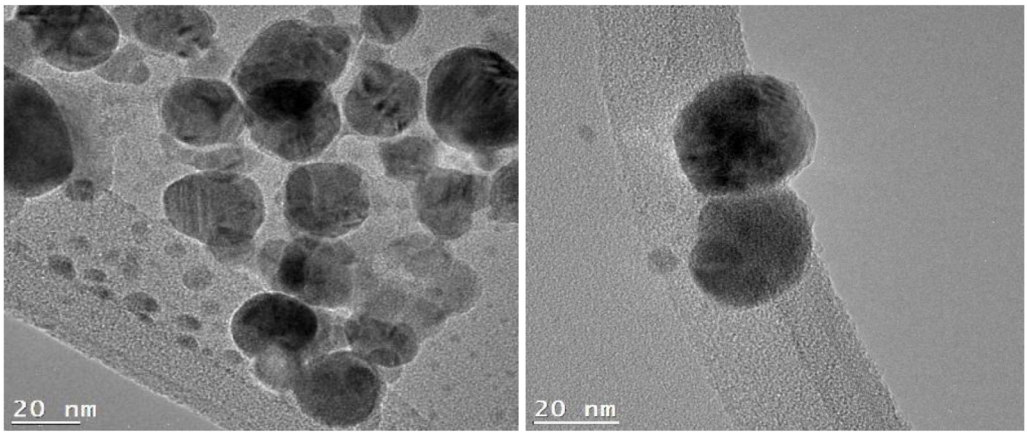

Fig. 4. Bright field transmission electron microscopic (TEM) images of Ag NPs obtained from the bulk Ag target in DI water *via* the LASiS technique.

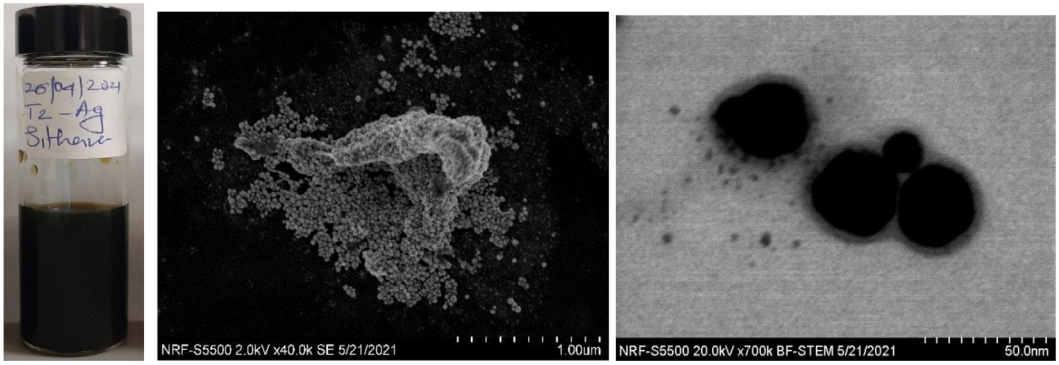

Fig. 5. (a) As-produced and centrifuge concentrated LASiS Ag colloids. (b) SE image and (c) Bright Field-STEM image of the centrifuged Ag colloid recorded using FE-SEM.

layer exhibited semiconductor like behaviour, with the resistance becoming measurable at high temperature and remaining in the MΩ range. The lack of significant hysteresis on increasing and decreasing the temperature in the heat-treatment stages suggests that the resistance is not improved *via* heat treatment.

The drop-cast layer produced with the centrifuge-concentrated Ag NP colloid (Fig. 7a inset) gave an initial room temperature resistance of 20 kΩ. The in-situ resistance measured during heat treatment is presented in Fig. 7a. The layer exhibits a semiconductor-like behaviour with the resistance decreasing as the temperature increases. This indicates the metallic NPs may have a shell of oxide or sulphide, which forms the interface between the particles, leading to domination of semiconductor behaviour. However, the concentration has improved the resistance compared to the as-produced ink, with the same volume of ink containing greater amounts of nanomaterial and reduced spreading, creating a more robust conductive path on the surface. Significant hysteresis begins in the 105–150 °C range, indicating the commencement of a permanent change in the conductivity. The initial resistance of 15.8 kΩ at 40 °C reached the lowest value of 60.2 Ω, reduced by over 99% of the initial resistance.

After heat treatment, the samples were allowed to cool in the nitrogen flow, then the first three heating stages (45–90, 65–110 and 85–130 °C) were repeated to observe any permanently changed resistance behaviour. Fig. 7b compares the first three stages (45–90, 65–110 and 85-130 °C) from Fig. 7a and the post-anneal repetition of these stages. The three plots in the lower half of Fig. 7b show the behaviour after annealing in the nitrogen flow. This illustrates the change in resistance has been permanent. The behaviour of the layer is now dominated by a slightly metallic behaviour – resistance increasing with temperature – indicating the heat treatment has promoted the formation of metal–metal connections between the NPs. However, the resistance is highly stable with temperature, ranging from 58.7 to 60.2 Ω over the temperature range 45–130 °C. The results indicate that by improving the concentration of colloid and annealing heat treatment of print structures, LASiS ink can be used for printed electronic application. The improvement in the resistance values of the centrifuge concentrated LASiS colloid may due to the reduced surface area of the agglomerated large particle that avoids unwanted oxidation when printing and the thicker layers that can be produced with the same ink volume.

4. Conclusions

Conductive inks are a low-cost way of applying conductive tracks and layers, and drop casting allows for simple characterization of the inks and their behaviour. In this work, the generation of Ag NP colloids using a dynamic flow based LASiS system capable of high production rates and the heat-treatment behaviour of drop-cast layers of concentrated Ag NP based ink are reported. Metallic Ag NP colloids were successfully produced with a concentration of $\sim$0.9 mg mL^{-1} and an average particle size

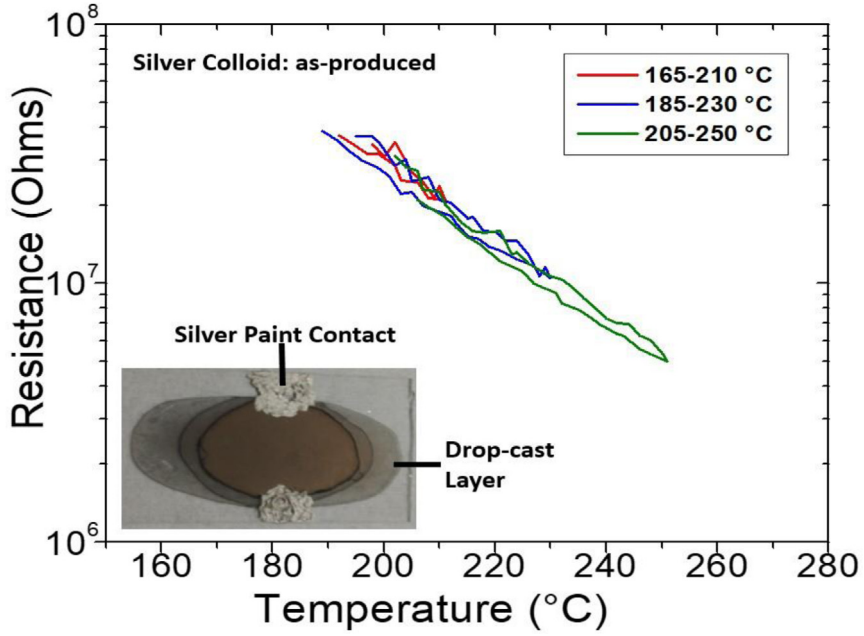

Fig. 6. In-situ resistance *vs.* temperature during heat-treatment for the drop-cast as-produced ink. Inset picture shows the as-produced silver ink drop-casting on a glass substrate.

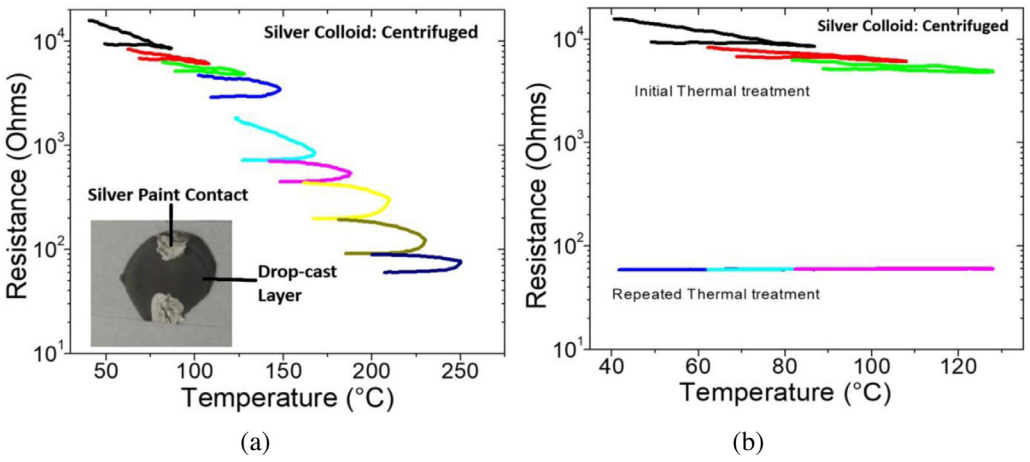

Fig. 7. (a) In-situ resistance vs. temperature during heat-treatment of the centrifuged ink drop-cast layer and (b) in-situ resistance *vs.* temperature during first three stages of the initial heat treatment and a repetition of these stages after the completed heat treatment.

of ∼34 ± 5 nm. The colloids were concentrated by centrifuging, removing a portion of the supernate and sonicating to re-suspend the particles. Simple drop-cast layers of the as-produced and concentrated LASiS Ag ink were heat-treated under a nitrogen flow while monitoring the resistance in-situ to characterize the Ag drop cast layer performance. The layers were found to give a high initial resistance with semiconductor-like behaviour, likely due to oxide formation during the drop-cast and drying process in air. Annealing the concentrated ink samples under a nitrogen flow was found to significantly improve the conductivity, beginning in the temperature range 105–150 °C. The heat-treatment allows the formation of more metal–metal conduction across the NP layer, leading to dominant metallic behaviour afterwards and significantly lowered resistance (from 20 to 60 Ω), as shown in Fig. 7b.

Inert gases to achieve good conductivity may negatively impact the ease-of-use for industrial applications. These results indicate good suitability for application in conductive inks, however there is a need for further study to investigate how different processing environments, including ambient conditions, affect the resulting conductivity and other physical properties.

CRediT authorship contribution statement

Éanna McCarthy: Conceptualization, Methodology. **Sithara Pavithran Sreenilayam:** Conceptualization, Methodology, Writing – original draft. **Oskar Ronan:** Experiment and reviewing. **Hasan Ayub:** Experiment. **Ronan McCann:** Experiment and reviewing. **Lorcan McKeon:** Experiment and reviewing. **Karsten Fleischer:** Conceptualization. **Valeria Nicolosi:** Writing – review & editing. **Dermot Brabazon:** Conceptualization, Supervision, Writing – review & editing.

Declaration of competing interest

The authors declare that they have no known competing financial interests or personal relationships that could have appeared to influence the work reported in this paper.

Acknowledgements

This work is supported in part by a research grant from Science Foundation Ireland (SFI) under Grant Numbers 16/1571 RC/3872 and 19/US-C2C/3579, and is co-funded under the European Regional Development Fund and by I-Form industry partners, Ireland and from the European Union's Horizon 2020 Research and Innovation Programme under grant agreement No. 862100. Authors wish to acknowledge the Advanced Microscopy Laboratory, Trinity College Dublin, Ireland for the use of their facilities.

References

[1] S.P. Sreenilayam, I.U. Ahad, V. Nicolosi, V.A. Garzon, D. Brabazon, Advanced materials of printed wearables for physiological parameter monitoring, Mater. Today 32 (2020) 147–177, https://doi.org/10.1016/j.mattod.2019.08.005.

[2] A. Verma, D. Martineau, S. Abdolhosseinzadeh, J. Heier, F. Nüesch, Inkjet printed mesoscopic perovskite solar cells with custom design capability, Mater. Adv. 1 (2020) 153160, https://doi.org/10.1039/D0MA00077A.

[3] https://www.marketsandmarkets.com/Market-Reports/conductive-ink-market154484169.html. (Accessed 05 August 2021).

[4] Q.J. Huang, W.F. Shen, W.J. Song, Synthesis of colourless silver precursor ink for printing conductive patterns on silicon nitride substrates, Appl. Surf. Sci. 258 (2012) 7384, https://doi.org/10.1016/j.apsusc.2012.04.037.

[5] G.C. Pidcock, Marc in het Panhuis, Extrusion printing: Extrusion printing of flexible electrically conducting carbon nanotube networks, Adv. Funct. Mater. 22 (2012) 4790–4800, https://doi.org/10.1002/adfm.201290133.

[6] S. Glatzel, Z. Schnepp, C. Giordano, From paper to structured carbon electrodes by inkjet printing, Angew. Chem. Int. Ed. 52 (2013) 2355–2358, https://doi.org/10.1002/anie.201207693.

[7] Z.T. Xiong, C.Q. Liu, Optimization of inkjet printed PEDOT:PSS thin films through annealing processes, Org. Electron. 13 (2012) 1532–1540, https://doi.org/10.1016/j.orgel.2012.05.005.

[8] L. Mo, D. Liu, W. Li, L. Li, L. Wang, X. Zhou, Effects of dodecylamine and dodecanethiol on the conductive properties of nano-ag films, Appl. Surf. Sci. 257 (2011) 5746–5753, https://doi.org/10.1016/j.apsusc.2011.01.090.

[9] M. Grouchko, A. Kamyshny, S. Magdassi, Formation of air-stable copper-silver core–shell nanoparticles for inkjet printing, J. Mater. Chem. 19 (2009) 3057–3062, https://doi.org/10.1039/B821327E.

[10] N. Zhao, M. Chiesa, H. Sirringhaus, Y. Li, Y. Wu, B. Ong, Self-aligned inkjet printing of highly conducting gold electrodes with submicron resolution, J. Appl. Phys. 101 (2007) 064513, https://doi.org/10.1063/1.2496249.

[11] M.K. Ahmed, A.A. Menazea, S.F. Mansour, Reem Al-Wafi, Differentiation between cellulose acetate and polyvinyl alcohol nanofibrous scaffolds containing magnetite nanoparticles/graphene oxide via pulsed laser ablation technique for tissue engineering applications, J. Mater. Res. Technol. 9 (2020) 11629–11640, https://doi.org/10.1016/j.jmrt.2020.08.041.

[12] P.P. Patil, D.M. Phase, S.A. Kulkarni, S.V. Ghaisas, S.K. Kulkarni, S.M. Kanetkar, S.B. Ogale, V.G. Bhide, Pulsed-laser –induced reactive quenching at liquid–solid interface: Aqueous oxidation of iron, Phys. Rev. Lett. 58 (1987) 238, https://doi.org/10.1103/PhysRevLett.58.238.

[13] J. Neddersen, G. Chumanov, T.M. Cotton, Laser ablation of metals: A new method for preparing SERS active colloids, Appl. Spectrosc. 47 (1993) 1959, https://doi.org/10.1366/0003702934066460.

[14] H. Zeng, X.-W. Du, S.C. Singh, S.A. Kulinich, S. Yang, J. He, W. Cai, Nanomaterials via laser ablation/irradiation in liquid: A review, Adv. Funct. Mater. 22 (2012) 1333, https://doi.org/10.1002/adfm.201102295.

[15] F. Mafune, J.-ya. Kohno, Y. Takeda, T. Kondow, H. Sawabe, Structure and stability of silver nanoparticles in aqueous solution produced by laser ablation, J. Phys. Chem. B 104 (2000) 8333, https://doi.org/10.1021/jp001803b.

[16] M.K. Ahmed, A.M. Moydeen, A.M. Ismail, M.E. El-Naggar, A.A. Menazea, M.H. El-Newehy, Wound dressing properties of functionalized environmentally biopolymer loaded with selenium nanoparticles, J. Mol. Struct. 1225 (2021) 129138, https://doi.org/10.1016/j.molstruc.2020.129138.

[17] A.A. Menazea, N.S. Awwad, Antibacterial activity of TiO2 doped ZnO composite synthesized via laser ablation route for antimicrobial application, J. Mater. Res. Technol. 9 (2020) 9434–9441, https://doi.org/10.1016/j.jmrt.2020.05.103.

[18] M.J. Tommalieh, H.A. Ibrahium, N.S. Awwad, A.A. Menazea, Gold nanoparticles doped polyvinyl alcohol/chitosan blend via laser ablation for electrical conductivity enhancement, J. Mol. Struct. 1221 (2020) 128814, https://doi.org/10.1016/j.molstruc.2020.128814.

[19] M.K. Ahmed, M.E. El-Naggar, A. Aldalbahi, M.H. El-Newehy, A.A. Menazea, Methylene blue degradation under visible light of metallic nanoparticles scattered into graphene oxide using laser ablation technique in aqueous solutions, J. Mol. Liq. 315 (2020) 113794, https://doi.org/10.1016/j.molliq.2020.113794.

[20] S.S. Pavithran, R. McCann, É. McCarthy, B. Freeland, K. Fleischer, S. Goodnick, S. Bowden, C. Honsberg, D. Brabazon, Silver and Copper nanocolloid generation via Pulsed Laser Ablation in Liquid: Recirculation nanoparticle production mode, in: Paper presented at ESAFORM 2021. 24th International Conference on Material Forming, Liège, Belgique. https://doi.org/10.25518/esaform21.2239.

[21] F. Correard, K. Maximova, M.-A. Estève, C. Villard, M. Roy, A. Al-Kattan, M. Sentis, M. Gingras, A.V. Kabashin, D. Braguer, Gold nanoparticles prepared by laser ablation in aqueous biocompatible solutions: assessment of safety and biological identity for nanomedicine applications, Int. J. Nanomed. 9 (2014) 5415–5430, https://doi.org/10.2147/IJN.S65817.

[22] D.E. Martínez-Tong, M. Sanz, T.A. Ezquerra, A. Nogales, J.F. Marco, M. Castillejo, E. Rebollar, Formation of polymer nanoparticles by UV pulsed laser ablation of poly (bisphenol A carbonate) in liquid environment, Appl. Surf. Sci. 418 (2017) 522–529, https://doi.org/10.1016/j.apsusc.2016.11.186.

[23] K.S. Khashan, R.A. Ismail, R.O. Mahdi, Synthesis of SiC nanoparticles by SHG 532 nm Nd:YAG laser ablation of silicon in ethanol, Appl. Phys. A 124 (2018) 443, https://doi.org/10.1007/s00339-018-1835-7.

[24] B. Freeland, R. McCann, P. O'Neill, S. Sreenilayam, M. Tiefenthaler, M. Dabros, M. Juillerat, G. Foley, D. Brabazon, Real-time monitoring and control for high-efficiency autonomous laser fabrication of silicon nanoparticle colloids, Int. J. Adv. Manuf. Technol. 114 (2021) 291–304, https://doi.org/10.1007/s00170-021-06772-6.

[25] H.B. Zeng, W. Cai, Y. Li, J. Hu, P. Liu, Composition/structural evolution and optical properties of ZnO/Zn nanoparticles by laser ablation in liquid media, J. Phys. Chem. B 109 (2005) 18260–18266, https://doi.org/10.1021/jp052258n.

[26] A. Al-Hamaoy, E. Chikarakara, H. Jawad, K. Gupta, D. Kumar, M.S.R. Rao, S. Krishnamurthy, M. Morshed, E. Fox, D. Brougham, X. He, M. Vázquez, D. Brabazon, Liquid phase – pulsed laser ablation: A route to fabricate different carbon nanostructures, Appl. Surf. Sci. 302 (2014) 141–144, https://doi.org/10.1016/j.apsusc.2013.09.102.

[27] M. Ocwieja, Z. Adamczyk, M. Morga, K. Kubiak, Silver particle monolayers formation, stability, applications, Adv. Colloid Interface Sci. 222 (2015) 530–563, https://doi.org/10.1016/j.cis.2014.07.001.

[28] R. Streubel, S. Barcikowski, B. Gökce, Continuous multigram nanoparticle synthesis by high-power, high-repetition-rate ultrafast laser ablation in liquids, Opt. Lett. 41 (2016) 1486, https://doi.org/10.1364/OL.41.001486.

[29] P. Wagener, A. Schwenke, B.N. Chichkov, S. Barcikowski, Pulsed laser ablation of zinc in tetrahydrofuran: Bypassing the cavitation bubble, J. Phys. Chem. C 114 (2010) 7618–7625, https://doi.org/10.1021/jp911243a.

[30] S. Barcikowski, F. Mafuné, Trends and current topics in the field of laser ablation and nanoparticle generation in liquids, J. Phys. Chem. C 115 (2011) 4985, https://doi.org/10.1021/jp111036a.

[31] S. Barcikowski, V. Amendola, G. Marzun, C. Rehbock, S. Reichenberger, D. Zhang, B. Gokce, Handbook of Laser Synthesis of Colloids, DuEPublico, 2016, https://doi.org/10.17185/duepublico/41087.

[32] https://www.cytodiagnostics.com/pages/silver-nanoparticle-properties. (Accessed 26 July 2021).

[33] M. Eslamian, F. Zabihi, Ultrasonic substrate vibration-assisted drop casting (SVADC) for the fabrication of photovoltaic solar cell arrays and thin-film devices, Nanoscale Res. Lett. 10 (2015) 462, https://doi.org/10.1186/s11671-015-1168-9.

[34] S.P. Sreenilayam, I. Ul Ahad, V. Nicolosi, D. Brabazon, Mxene materials based printed flexible devices for healthcare, biomedical and energy storage applications, Mater. Today 43 (2021) 99–131, https://doi.org/10.1016/j.mattod.2020.10.025.

[35] A. Kosmala, R. Wright, Q. Zhang, P. Kirby, Synthesis of silver nano particles and fabrication of aqueous Ag inks for inkjet printing, Mater. Chem. Phys. 129 (2011) 1075–1080, https://doi.org/10.1016/j.matchemphys.2011.05.064.

[36] Y.Z. Zhao, D.X. Du, Y.H. Wang, Preparation of silver nanoparticles and application in water-based conductive inks, Internat. J. Modern Phys. B 33 (2019) 1950385, https://doi.org/10.1142/S0217979219503855.

[37] Z. Zhang, T. Si, J. Liu, Controllable assembly of a hierarchical multiscale architecture based on silver nanoparticle grids/nanowires for flexible organic solar cells, Nanotechnology 29 (2018) 415603, https://doi.org/10.1088/1361-6528/aad6aa.

[38] K. Bagga, R. McCann, Q. Brasi, J. Coussy, A. Stalcup, M. Vázquez, D. Brabazon, Laserassisted synthesis of ultrapure nanostructures for biological sensing applications, in: Proceedings Volume 9928, Nanobiosystems: Processing, Characterization, and Applications IX; 99280O Event: SPIE Nanoscience Engineering, San Diego, California, United States, 2016, https://doi.org/10.1117/12.2237147.

[39] Y. Al-Douri, R.A. Al-Samarai, S.A. Abdulateef, Ali.Abu. Odeh, N. Badih, C.H. Voon, Nanosecond pulsed laser ablation to synthesize GaO colloidal nanoparticles: Optical and structural properties, Optik 178 (2019) 337–342338, https://doi.org/10.1016/j.ijleo.2018.09.158.

[40] Y. Al-Douri, S.A. Abdulateef, Ali.Abu. Odeh, C.H. Voon, N. Badi, GaNO colloidal nanoparticles synthesis by nanosecond pulsed laser ablation: Laser fluence dependent optical absorption and structural properties, Powder Technol. 320 (2017) 457–461, https://doi.org/10.1016/j.powtec.2017.07.059.

[41] Y. Al-Douri, Nanosecond Pulsed Laser Ablation To Synthesize Ternary Alloy Colloidal Nanoparticles, Colloidal Metal Oxide Nanoparticles Synthesis, Characterization and Applications, Metal Oxides, 1st ed., Elsevier, 2020, pp. 25–38, https://doi.org/10.1016/b978-0-12-813357-6.00003-6, Chapter 3.

[42] R.A. Ismail, G.M. Sulaiman, M.H. Mohsin, A.H. Saadoon, Preparation of silver iodide nanoparticles using laser ablation in liquid for antibacterial applications, IET Nanobiotechnol. 12 (2018) 781–786, https://doi.org/10.1049/iet-nbt.2017.0231.

[43] K.S. Khashan, G.M. Sulaiman, R. Mahdi, A. kadhim, The effect of laser energy on the properties of carbon nanotube—iron oxide nanoparticles composite prepared via pulsed laser ablation in liquid, Mater. Res. Express 5 (2018) 105004, https://doi.org/10.1088/2053-1591/aadabc.